ACS Sustainable Chemistry & Engineering

pubs.acs.org/journal/ascecg

Research Article

Assessing the Performance Limits of Electrochemical CO_2 Separation Using Exergy Loss Analysis and Zero-Dimensional Modeling

Fawaz Ali, Sanat Modak, and David G. Kwabi*

Cite This: *ACS Sustainable Chem. Eng.* 2023, 11, 16995−17005

Read Online

ACCESS | Metrics & More | Article Recommendations | Supporting Information

ABSTRACT: Electrochemical CO_2 separation is drawing attention as a promising strategy for using renewable energy to mitigate climate change. Several studies have shown that the minimum energy input thermodynamically required for such separation, either via pH-swing or nucleophilic binding of CO_2 to a charge carrier, can be very low (<100 kJ $mol_{CO_2}^{-1}$). Nevertheless, understanding how measured energetic costs are likely to vary as a function of various electrochemical and separation process parameters in practical applications is not fully understood. In this study, we first show that the minimum energy required to execute any electrochemical CO_2 separation cycle is a function of the exergy losses incurred by the entry of CO_2 into the electrolyte (from a dilute inlet feed) or the release of CO_2 from the electrolyte (into a more concentrated exit stream). These exergy losses can be calculated based on the trajectories of solution- and gas-phase concentrations of CO_2 throughout a given separation cycle; they do not depend on the separation mechanism (i.e., whether related to pH-swing or direct binding of CO_2 to a nucleophilic charge carrier). Then, we develop a zero-dimensional model of pH-swing-driven CO_2 separation in a flow cell, which incorporates the physics of reactive CO_2 capture into alkaline media with the cell's electrochemical operation. From the output of the model, we show how the overall energetic cost of separation can be decomposed into distinct contributions arising from exergy and other flow cell-specific losses (i.e., to interfacial charge transfer, mass transport, and Ohmic resistance of the cell). Variations in energetic cost as a function of CO_2 removed, current density, and the rate constant of CO_2 hydroxylation are explored. Our investigations reveal that when CO_2 capture is rate-limiting for the overall separation process, the trade-off/relationship between energy input and the CO_2 throughput is strongly dictated by the difference between the time allotted for CO_2 invasion during cycling and the time required for reactive capture of CO_2. When those timescales are comparable, the energy input and CO_2 throughput are optimally low and high, respectively. Our work contributes toward ongoing efforts to design electrochemical systems that could meet the techno-economic requirements for practically viable CO_2 separation.

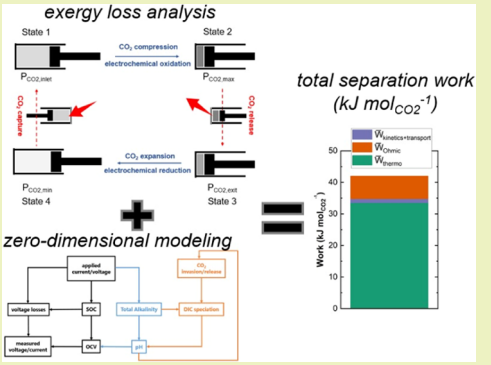

KEYWORDS: *exergy, CO_2 capture, CO_2 release, pH swing, CO_2 productivity*

INTRODUCTION

CO_2 emissions from fossil fuel combustion have increased sharply since the Industrial Revolution, resulting in a rapid rise in global average temperatures and a disruption in long-standing climate patterns.[1,2] Unfortunately, the societal transition away from fossil fuels to renewable or otherwise carbon-neutral sources of energy is not occurring rapidly enough to avoid the most severe consequences of climate change, and certain energy sectors may prove too difficult to substantially decarbonize in the short term. Recent climate models indicate that stabilizing average global temperatures to <2 °C higher than in the preindustrial era is likely to require CO_2 capture, from ∼10 Gt/year by midcentury to 20 Gt/year by the end of the century.[3] Separation and sequestration of CO_2 from point sources, and natural sinks such as the atmosphere and oceans, is therefore becoming an essential and urgently required strategy for climate change mitigation.[4,5]

The most established methods of CO_2 separation involve reactive capture using strongly nucleophilic or alkaline sorbents, followed by thermal regeneration of the sorbent at high temperatures and simultaneous release of pure CO_2. Various embodiments of this cycle have been demonstrated using amines and caustic soda (>2 M NaOH) for CO_2 capture from flue gas[6] and air,[7] respectively. Unfortunately, the need for high-temperature (between 200 and 900 °C) heat for sorbent regeneration poses some practical and fundamental challenges to widespread implementation. Practically, high-temperature heat is most conveniently provided by fossil fuel

Received: August 2, 2023
Revised: November 4, 2023
Accepted: November 5, 2023
Published: November 21, 2023

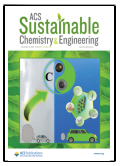

https://doi.org/10.1021/acssuschemeng.3c04867
ACS Sustainable Chem. Eng. 2023, 11, 16995−17005

combustion. This imposes additional energetic costs, either to co-capture the additional CO_2 or to separate oxygen from air for oxy-fuel combustion. More fundamentally, the energy efficiency of heat-to-work separation faces an intrinsic (Carnot) limit that is less than unity,[8] which results in high thermal energy costs, up to 390 kJ $mol_{CO_2}^{-1}$ for direct air capture (DAC) of CO_2 in pilot-scale plants.[7]

Electrochemical strategies for CO_2 separation[9] are attractive because they are not subject to a Carnot efficiency limit and may run directly on renewable electricity, which is becoming increasingly inexpensive. Many approaches for electrochemical CO_2 capture from flue gas, air, and seawater have been proposed, with the vast majority of them falling under two broad categories: (1) pH swing/gradient methods, which take advantage of the disparate aqueous solubilities of (bi)-carbonate ions and neutral CO_2, and their pH-dependent speciation,[10−15] and (2) reversible nucleophilic binding between redox-active sorbents or sorbent mediators, and CO_2.[16−19]

Attention has recently been paid to modeling how the minimum work thermodynamically required to execute a given separation cycle depends on such factors as binding energetics of the sorbent to CO_2, and the degree to which solution-phase CO_2 is allowed to equilibrate with CO_2 in the gas phase.[10,20−22] These studies have also shed light on sorbent solubilities that would be required for CO_2 separation from air vs flue gas, and trade-offs between thermodynamic efficiency and sorbent utilization.[23] It is typically assumed in these reports, however, that at every step in the separation cycle, sorbent-bound CO_2 exists either in equilibrium with its gas-phase concentration or in complete disequilibrium. The resulting minimum work then depends on the combination of binary choices adopted for each step of a given separation cycle. In practice, the degree to which CO_2 equilibrates with its gas-phase composition will vary along the spectrum between these two extremes and will depend on the timescale required for the release or reactive capture of CO_2 compared to that for redox cycling or activation/regeneration of the sorbent. How these timescales compare will depend on whether a pH-swing or nucleophilic binding approach is used, the relevant sorbent-CO_2 binding energetics and kinetics, and whether a homogeneous catalyst is present, among other factors. As such, there is a need to understand how the minimum CO_2 separation work will vary in situations where partial equilibration between gas- and liquid-phase CO_2 is allowed. Beyond analyses of minimum work, there is also a pressing need to understand how additional kinetic losses necessary to drive a specific current density contribute to the total separation work that would be measured in real electrochemical systems. Understanding how this total work varies as a function of separation process parameters (e.g., partial pressure of the CO_2 feed and the fraction of CO_2 removed from it), the properties of the electrochemical cell, and the cycling protocol is critical for designing electrochemical CO_2 separation for high energy efficiencies at acceptable throughputs.

The Second Law of Thermodynamics requires that the minimum work of electrochemical CO_2 separation over a given cycle is the sum of the net increase in the level of CO_2 exergy and exergy losses incurred during CO_2 capture and release. This requirement applies regardless of the mechanism for CO_2 capture (i.e., whether based on pH swing or nucleophilic binding), and provides a context within which the influence of a fluctuating CO_2 equilibrium on the minimum work can be discerned. In this work, we derive expressions for the exergy losses based on the trajectories of solution- and gas-phase $[CO_2]$ and demonstrate that they reveal constraints on certain physicochemical properties (pK_a, CO_2 binding constant, and solubility) of molecules that could enact CO_2 separation. Then, by modifying a zero-dimensional model that we have recently developed for organic flow batteries,[24] we also simulate the total work required for pH-swing-driven CO_2 separation from flue gas and air using proton-coupled electron transfer (PCET).[10,11,25] We show that this work is readily understood in terms of distinct contributions from thermodynamic and kinetic (including exergy) losses. Our results provide guidelines for designing high-efficiency, high-throughput electrochemical CO_2 separation systems and add to the growing body of research demonstrating the utility of exergy loss/entropy generation analysis for applications in energy storage and chemical separations.[26,27]

RESULTS AND DISCUSSION

Theoretical Considerations. Regardless of the electrochemical CO_2 separation mechanism (i.e., whether related to pH swing or nucleophilic binding to CO_2), the minimum work thermodynamically required to separate CO_2, $\bar{W}_{thermo}$ (kJ $mol_{CO_2}^{-1}$), is the sum of the net increase in CO_2 exergy and exergy losses incurred over the course of a separation cycle. Exergy is the maximum useful work that is theoretically recoverable from a system with respect to its environment. The separation of CO_2 increases its exergy because it is concentrated from lower to higher partial pressure (P_{CO_2}) or pCO_2. The minimum theoretical work required for this increase in exergy at a constant temperature ($\bar{W}_{min,theor}$) is the absolute difference in the free energy of CO_2 between its dilute and concentrated states. Assuming an infinite CO_2 source (inlet) and sink (exit), $\bar{W}_{min,theor}$ is defined as[28]

$$\bar{W}_{min,theor} = RT \ln \frac{P_{CO_2,exit}}{P_{CO_2,inlet}} \quad (1)$$

Here, CO_2 is absorbed from an inlet gas reservoir with a CO_2 partial pressure of $P_{CO_2,inlet}$, concentrated, and released to an exit reservoir at partial pressure $P_{CO_2,exit}$; R and T are the universal gas constant (8.314 J mol^{-1} K^{-1}) and temperature (in K), respectively. The derivation of and expression for $\bar{W}_{min,theor}$ with a finite-sized inlet (feed) reservoir are given, respectively, in eqs S1−S8 and eq S9. A cycle consuming $\bar{W}_{min,theor}$will proceed at an infinitesimal rate because there would be no finite gradients in the chemical potential of CO_2 at the system's boundary to drive CO_2 capture or release. The difference between $\bar{W}_{min,theor}$ and the minimum work that is thermodynamically required for a cycle where such gradients may exist ($\bar{W}_{thermo}$) represents the energy penalty for driving CO_2 capture and release at finite rates. Those rates will increase with increasing $\bar{W}_{thermo} - \bar{W}_{min,theor}$, resulting in a trade-off between the energetic cost and throughput of CO_2 separation.

As applied to electrochemical CO_2 separation, the above argument may be developed by analogizing the electrochemical cell as a hypothetical mechanical piston−cylinder system with cylinder walls that can alternate between being permeable to CO_2 and non-CO_2 components of any gas composition

https://doi.org/10.1021/acssuschemeng.3c04867
ACS Sustainable Chem. Eng. 2023, 11, 16995−17005

(Figure 1). The compression step (1 → 2) in Figure 1 corresponds to an increase in the activity of CO_2 or, assuming

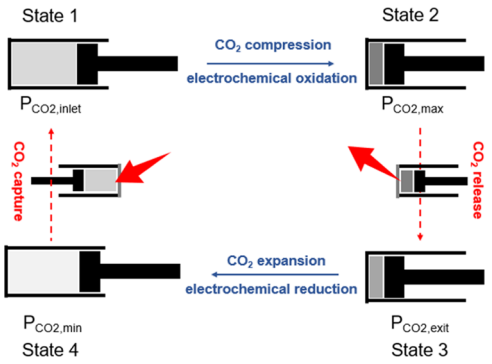

Figure 1. Hypothetical four-step CO_2 separation cycle using a mechanical piston−cylinder system as an analogue of an electrochemical cell. The partial pressure of CO_2 in the system is $P_{CO_2,inlet}$ at State 1; after compression, it is $P_{CO_2,max}$ (State 2). CO_2 release to the exit then occurs until the system reaches $P_{CO_2,exit}$, after which expansion results in a decrease to $P_{CO_2,min}$. CO_2 capture then completes the cycle. The compression and expansion steps (blue arrows) correspond to the electrochemical reduction or oxidation of a redox-active electrolyte, resulting in changes to $[CO_2]$. During these steps, the cylinder is permeable only to non-CO_2 gases. Exergy losses occur during the CO_2 release and capture steps (red arrows), where the cylinder is made permeable only to CO_2. Note that $P_{CO_2,max} \geq P_{CO_2,exit} > P_{CO_2,inlet} \geq P_{CO_2,min}$.

ideality, P_{CO2}. Such an increase would be caused, for pH-swing-based separation, by electrochemically driven conversion of (bi)carbonate species to neutral CO_2, or for nucleophilic binding (NB)-based separation, by conversion of a CO_2-bound redox species to a redox state with low affinity for CO_2. The expansion step (3 → 4) corresponds to the reverse of this process. CO_2 capture into (4 → 1) or release (2 → 3) from the system occurs in response to expansion or compression in accordance with the gradient in P_{CO_2} at the system boundary. CO_2 separation cycles in which the compression and release steps as well as the expansion and capture steps occur separately comprise four steps. In a three-step cycle, either CO_2 compression and release or CO_2 expansion and capture are combined into one step. In a two-step cycle, CO_2 compression and expansion are combined with CO_2 release and capture, respectively.[10,23]

In steps 2 → 3 (CO_2 release) and 4 → 1 (CO_2 capture), there is a loss of stream exergy by virtue of the throttled release or entry of CO_2 from or into the system. These exergy losses (i.e., $\bar{W}_{thermo} - \bar{W}_{min,theor}$) are equal to the total reversible work that might have been transferred by the flow of CO_2, for instance, by a hypothetical isothermal turbine interposed between the system and the environment. Calculating this reversible work yields $\bar{W}_{thermo} - \bar{W}_{min,theor}$. $\bar{W}_{thermo}$ may therefore be computed by calculating $\bar{W}_{min,theor}$ based on eqs 1 or S9. Following our previous work,[10] we define the ratio between the maximum pressure of CO_2 after compression ($P_{CO_2,max}$) and the partial pressure of CO_2 within the reservoir to which it is released ($P_{CO_2,exit}$), as the outgassing overpressure (OP). Analogously, the ratio between the minimum pressure of CO_2 immediately preceding CO_2 capture ($P_{CO_2,min}$) and the partial pressure of CO_2 within the inlet feed ($P_{CO_2,inlet}$), is defined as the invasion underpressure (IU).

$\bar{W}_{thermo}$ computed via exergy loss analysis is identical to the total work transferred by the piston over a cycle ($\bar{W}_{mechanical}$), and may be expressed as

$$\bar{W}_{thermo} = \bar{W}_{min,theor} + \bar{W}_{exergy,release} + \bar{W}_{exergy,capture} \quad (2)$$

where $\bar{W}_{exergy,release}$ and $\bar{W}_{exergy,capture}$ are the exergy losses during steps 2 → 3 and 4 → 1, respectively. In Section S2, we demonstrate analytically that for any cycle in which IU = 1, $\bar{W}_{mechanical} = \bar{W}_{thermo}$ and also that $\bar{W}_{exergy,release}$ is a function of OP (eq S40).

Minimum Energetic Cost of Electrochemical CO_2 Separation Using Exergy Loss Analysis. Because $\bar{W}_{thermo}$ is the total work transferred by the piston, it is also the total electrical work transferred by an electrochemical cell ($\bar{W}_{echem}$) in the analogous separation process. This result is an outcome of the Second Law of Thermodynamics and should hold regardless of the mechanism for CO_2 capture (pH-swing or NB), and whether or not the compression/expansion steps are separated from or combined with the CO_2 capture/release steps in two- or three-step cycles.[10,21,23]

To demonstrate the identity between $\bar{W}_{thermo}$ and $\bar{W}_{echem}$ we computed both quantities via exergy loss analysis and electrochemical models for CO_2 separation via pH-swing driven by PCET[10] and via NB.[21,23] Models describing the relationship among electrode potential, the state-of-charge (SOC) of the electrolyte, dissolved inorganic carbon (DIC), and $[CO_2]$ have been comprehensively described in previous work,[10,21,23] and important details are recapitulated in Section S3. A snapshot of the models' results is shown in Figure S1, which reports electrode potential and $[CO_2]$ vs SOC, respectively, for four-step cycles of pH-swing (Figure S1a,b)- and NB (Figure S1c,d)-driven CO_2 separation from 410 ppm to 1 bar. By taking the cyclic integrals of the potential vs SOC curves, we calculated $\bar{W}_{echem}$ according to

$$\bar{W}_{echem} = \frac{nF[Q_0]}{\Delta DIC_{released}} \oint E \, dSOC \quad (3)$$

where n and $[Q_0]$ are the number of transferrable electrons for and the total concentration, respectively, of the redox-active molecule, and F is Faraday's constant (96,485 C mol^{-1}). For the pH-swing simulation, $[Q_0]$ = 1.0 M and $2H^+$, $2e^-$ PCET was assumed to occur at all pH values. The resulting OP and IU were 31.2 and 6.56 × 10^9, respectively. For the NB simulation, $[Q_0]$ = 0.36 M and the binding constant of the reduced form of the molecule to CO_2 (K_b) was such that $\log(K_b)$ = 5.43, and OP and IU were 10 and 1000, respectively. $\bar{W}_{echem}$ was calculated according to eq 3 to be 67.1 and 34.1 kJ $mol_{CO_2}^{-1}$ for the four-step pH-swing and NB cases, respectively, and these figures were identical to $\bar{W}_{thermo}$ calculated by using eq 2. Figure S2 shows similar results for simulations of CO_2 separation from 0.05 to 1 bar. The agreement between $\bar{W}_{thermo}$ and $\bar{W}_{echem}$ extended to two- and three-step cycles that enacted capture from 410 ppm (Figure S3) and 0.05 bar (Figure S4).

Because $\bar{W}_{echem} = \bar{W}_{thermo}$, exergy loss analysis permits decomposition of $\bar{W}_{echem}$ into contributions from $\bar{W}_{min,theor}$, $\bar{W}_{exergy,capture}$, and $\bar{W}_{exergy,release}$. Understanding how these components vary with the $P_{CO_2,exit}/P_{CO_2,inlet}$ ratio, IU, OP, and other process parameters is important for designing

https://doi.org/10.1021/acssuschemeng.3c04867
ACS Sustainable Chem. Eng. 2023, 11, 16995−17005

separation schemes that optimize the trade-off between the energetic cost and rate of separation, and for evaluating $\bar{W}_{thermo}$ in experimental measurements. Exergy loss analysis also allows one to determine, given a minimum permissible $\bar{W}_{thermo}$, whether the pH swing or NB might be more appropriate for CO_2 separation. Such a situation may arise if techno-economic considerations dictate that CO_2 separation proceeds at a minimum flux. This minimum flux could translate to a maximum or minimum $[CO_2]$ in the sorbent during capture or release, from which a minimum $\bar{W}_{thermo}$ can be computed via eqs S13 and S17.

A minimum permissible $\bar{W}_{thermo}$ imposes constraints on the molecular properties required to execute the CO_2 separation. Figure 2 presents the relationship between the pH after

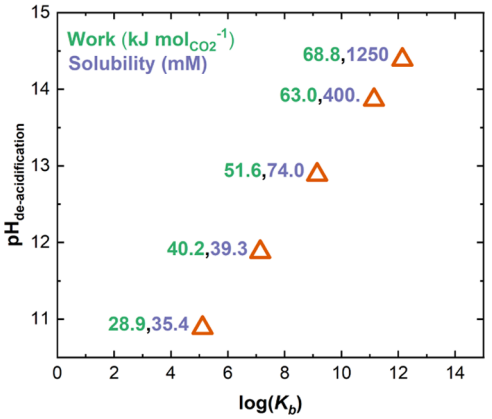

Figure 2. $pH_{deacidification}$ and $\log(K_b)$ for pH-swing- and NB-driven capture, respectively, for three-step electrochemical CO_2 separation cycles (with OP = 1) that yield the same $\bar{W}_{thermo}$ for CO_2 capture from 410 ppm and release to 1 bar.

deacidification ($pH_{deacidification}$) for pH-swing capture (State 4 in Figure 1) in a three-step cycle with OP = 1, and the CO_2-binding constant for NB-based capture that would result in the same $\bar{W}_{thermo}$. CO_2 is separated from an inlet feed of 410 ppm (i.e., P_{CO_2} in atmosphere) and IU ranges between 10^3 and 10^{10}. Because $\bar{W}_{echem} = \bar{W}_{thermo}$, $\bar{W}_{thermo}$ was calculated according to eq 3. We also considered the separation of CO_2 from 0.05 bar (Figure S5) to simulate flue gas capture. $\bar{W}_{thermo}$ (in green) and minimum solubilities for the PCET-active molecule (in purple) are indicated on the plots and lists of simulated data points are reported in Table S1 and Table S2 for capture from 410 ppm and 0.05 bar, respectively. For the NB simulations reported in Figures 2 and S5, a total molecular concentration of 0.71 M was used.

Because the pK_a of the reduced PCET-active agent must be equal to or greater than $pH_{deacidification}$ for alkalization to that pH to be possible, the y-axes of Figures 2 and S5 also indicate the minimum pK_a necessary to achieve the $\bar{W}_{thermo}$ indicated for CO_2 capture via pH swing. Based on Figure 2, a DAC cycle that is required to consume a $\bar{W}_{thermo}$ of at least 68.8 kJ $mol_{CO_2}^{-1}$ (the highest $\bar{W}_{thermo}$ considered) can only be enacted by a pH swing using a PCET-active molecule with a reduced-form pK_a and solubility of at least 14.4 and 1.25 M, respectively.

Quinone derivatives such as 4,5-dihydroxybenzene-1,3-disulfonic acid (also known as Tiron, solubility = 3 M at pH 0), and 3,6-dihydroxy-2,4-dimethylbenzenesulfonic acid (solubility = 2 M at pH 0) appear to satisfy the solubility requirement,[29] and Tiron has been deployed for pH-swing-driven CO_2 capture.[30,31] Nevertheless, it has an estimated pK_a of ~9,[31] which is too low, and it is prone to rapid decomposition in its oxidized form.[32] Other quinone derivatives have excellent stability,[33,34] but have solubilities around 1 M or lower. The prospects for finding an ideal quinone are slim, as most quinones are expected to possess reduced-form pK_a values lower than 12.[35] Phenazines are a different class of PCET-active molecules that have been deployed for CO_2 capture via pH swing.[10,11,15,25] Neutral Red, for instance, was recently revealed to exhibit oxygen-stable CO_2 capture capabilities, but has a reduced-form pK_a of 6.9.[15] Other phenazine derivatives[36−38] have higher pK_a values (up to 14), and solubilities between 1 and 1.8 M under alkaline conditions, and thus apparently fare better on the solubility and pK_a criteria. Nevertheless, their solubilities tend to be strongly dependent on the pH and choice of supporting electrolyte, and more extensive studies of pH-dependent solubility would be necessary to establish their suitability for DAC.

On the other hand, the $\bar{W}_{thermo}$ of 68.8 kJ $mol_{CO_2}^{-1}$ can be used to drive a DAC cycle via NB if $\log(K_b) > 12$, with the only constraint on molecular solubility being that it affords a greater concentration of CO_2-bound charge carriers than the solubility of CO_2 at the 1 bar exit stream (i.e., $P_{CO_2,max} > P_{CO_2,exit}$). This constraint translates to $K_b P_{CO_2,exit}[Q^-] > [CO_2]_{1\ bar}$, where $[Q^-]$ is the concentration of reduced but CO_2-free charge carriers at State 2. We found that this requirement is satisfied with our assumed molecular solubility of 0.71 M and $\log(K_b) > 3$ for a CO_2 solubility of 0.28 M at 1 bar, the highest solubility we are aware of (in acetonitrile[39]) for CO_2 among solvents that have been considered for NB-driven capture.[40] Several NB-active molecules that have been introduced in past studies have solubilities and CO_2-binding coefficients that render them suitable, such as 4,4′-azopyridine (solubility = 1.18 M in dimethyl sulfoxide, $\log(K_b) = 12.8$)[41] and 2,6-di-*tert*-butyl-1,4-benzoquinone (solubility > 0.43 M in dimethylformamide,[40] $\log(K_b) = 15$[42]); this is especially so given that the solubility of CO_2 is lower than 0.28 M in many other solvents, besides acetonitrile, that are appropriate for electrochemical applications (e.g., 0.18 M in dimethylformamide,[43] 0.14 M in dimethyl sulfoxide, and 0.13 M in propylene carbonate[40]). It follows that for a DAC cycle with a minimum $\bar{W}_{thermo}$ at the upper end of the range considered in Figure 2, NB- rather than pH-swing-driven capture is likely to be more practically feasible, provided it is possible to stabilize the molecule(s) used against oxidation by O_2 in air.[44]

Zero-Dimensional Model of pH-Swing-Driven CO_2 Separation. Having established the fundamental importance of exergy loss in governing the minimum energetic cost of any electrochemical CO_2 separation cycle, we now turn to how the total energetic cost of CO_2 separation may vary in operating cells. In addition to the exergy losses described above, any electrochemical system will consume extra work to drive a specific current. This additional work, which we denote hereafter as a cell loss,[a] may be required to overcome an Ohmic series resistance (e.g., due to the resistance of the membrane), and to drive interfacial charge transfer and mass transport.[45] Understanding how cell and exergy losses compose the total work, and the relationship between this total work and the rate of CO_2 capture, is critical for the design of electrochemical CO_2 separation systems that optimize the

https://doi.org/10.1021/acssuschemeng.3c04867
ACS Sustainable Chem. Eng. 2023, 11, 16995−17005

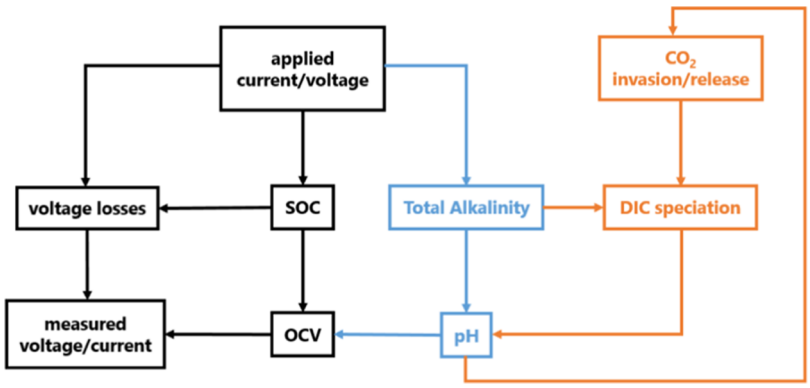

Figure 3. Conceptual illustration of the interactions among variables/processes relevant to electrochemical cycling of a flow cell (in black), pH swing (in blue), and the kinetics of CO_2 capture or release (in orange).

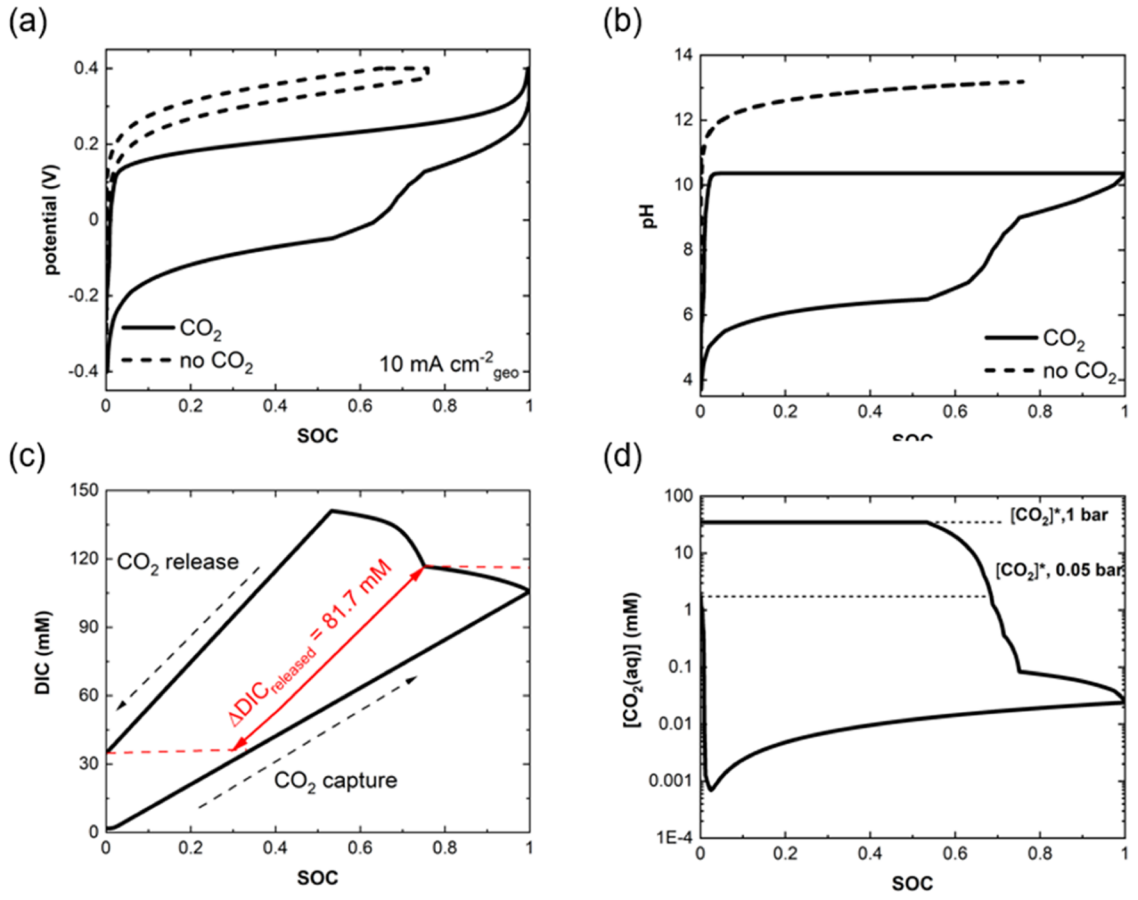

Figure 4. (a) Potential, (b) pH, (c) DIC, and (d) $[CO_2]$ vs SOC during CCCV cycling at 10 mA cm^{-2}. Dashed and solid lines correspond to simulations in the absence and presence of CO_2, respectively. The net DIC separated is indicated in (c), and $[CO_2]$* at 0.05 and 1 bar are indicated in (d).

trade-off between the energetic cost and rate of CO_2 separation. From a modeling perspective, this task is challenging because the voltage−current relationship—from which total work is calculated—is the result of a complex interplay among several dynamic variables/processes, which are schematically illustrated in Figure 3 for a pH-swing separation cycle driven by PCET. Here, the applied current determines not only the cell's voltage losses but also the rate of change of the electrolyte's SOC and total alkalinity (TA).[46] The electrolyte's TA regulates its DIC speciation and pH, but the pH determines the open-circuit potential of the cell—via the Nernst Equation—and the kinetics of reactive CO_2 capture or release, which in turn influences the trajectory of DIC. Any model that considers these dynamic, recursive relationships must also accommodate the numerical stiffness induced by widely varying timescales at which different processes can occur (e.g., CO_2 capture occurring more slowly than the rate of change of SOC).

We addressed this challenge by modifying a zero-dimensional electrochemical model recently developed by us of capacity fade in organic redox-flow batteries.[24] While the previous model considered the interaction between electrolyte

https://doi.org/10.1021/acssuschemeng.3c04867
ACS Sustainable Chem. Eng. 2023, 11, 16995−17005

decomposition and capacity retention, the model in this study examines the impact of changes in the electrolyte's composition (pH, DIC, and SOC) from electrochemical PCET and CO_2 capture/release on the total energetic cost and rate of CO_2 separation. The model system was a flow cell with a 7 mL capacity-limiting electrolyte (CLE) containing 158 mM of a molecule active for a $1e^-$, $1H^+$ PCET reaction ($Q + e^- + H^+ \leftrightarrow QH$), and a 40 mL non-capacity-limiting electrolyte (NCLE) comprising 200 mM of the same molecule but without the PCET activity. We assumed a Nernstian relationship between pH and the open-circuit potential of the CLE (eq S47). Voltage losses due to an Ohmic series resistance and mass transport were considered, and losses from interfacial charge transfer were governed by Butler–Volmer kinetics, as outlined in our previous work (eq S50).[24]

CO_2 capture and release were assumed to occur at the interfacial contact area between the CLE and its headspace gas ($A_{contact}$), with the capture step rate-limited by liquid-phase diffusion of CO_2 and reaction with OH^-.[47,48] Assuming the pH within the electrolyte is spatially homogeneous, and that aqueous CO_2, HCO_3^- and CO_3^{2-} are in equilibrium, this rate ($R_{capture}$, in mol s^{-1}) is[49]

$$R_{capture} = [CO_2]^* A_{contact} \sqrt{D_{CO_2} k_{OH^-} [OH^-]} \quad (4)$$

where $[CO_2]^*$ is the aqueous concentration of CO_2 in equilibrium with the gas-phase partial pressure of CO_2, D_{CO_2} is the diffusivity of CO_2 in water (1.2×10^{-5} cm^2 s^{-1}), and k_{OH^-} is the bimolecular rate constant of CO_2 hydroxylation ($CO_2 + OH^- \leftrightarrow HCO_3^-$). Henry's law dictates that $[CO_2]^* = P_{CO_2,inlet} \times H$, where H is Henry's law constant for CO_2 in water (35 mM bar^{-1}). CO_2 release was assumed to occur via physical desorption when $[CO_2] < [CO_2]^*$ at a rate ($R_{release}$) governed by the mass transport coefficient of CO_2, k_L:[49]

$$R_{release} = -k_L A_{contact} ([CO_2] - [CO_2]^*) \quad (5)$$

Figure 4 shows the simulated cell potential, pH, $[CO_2]$ and DIC for a baseline constant-current, constant-voltage (CCCV) cycle in the absence and presence of 0.05 bar of CO_2 at an applied current density of 10 mA cm^{-2}. Each half-cycle terminated once the voltage hit ±0.4 V and the current density during the CV step decayed to 1 mA cm^{-2}. Charge and discharge correspond to reduction and oxidation of the CLE, and deacidification/CO_2 capture and acidification/CO_2 release via appropriate changes in TA, respectively. Parameters describing the electrochemical properties of the flow cell and CO_2 capture/release kinetics are summarized in Table S3. In the absence of CO_2, the voltage hysteresis between charge and discharge (Figure 4a) is due only to cell losses, whereas there is no hysteresis in the pH vs SOC profile as expected (Figure 4b). In the CO_2-concentrating cycle, we assumed that the CLE was exposed to a feed CO_2 gas at 0.05 bar during charge, and then to 1 bar during discharge once the pH dropped below 9 (at which point $[CO_2] < [CO_2]^*$). Upon charge, the DIC increased steadily with increasing SOC, from 1.81 mM at SOC = 0.01 to 106 mM at SOC = 0.99. The switch from CO_2 partial pressure of 0.05 to 1 bar during discharge incurred a spike in DIC because $[CO_2] < [CO_2]^*$, but at SOC = 0.75, $[CO_2] > [CO_2]^*$ and CO_2 release was so rapid that $[CO_2]$ and $[CO_2]^*$ were nearly identical for the rest of the discharge half-cycle and $\bar{W}_{exergy,release}$ = 0.002 kJ $mol_{CO_2}^{-1}$. The negligible exergy loss during the release of CO_2 is a consequence of the high values assumed for k_L (0.05 cm s^{-1}), and $A_{contact}$ (48 cm^2), which enhance mass transfer of CO_2 from the solution to the gas phase. In situations where substantially lower values for k_L and $A_{contact}$ are expected, or there are other factors retarding CO_2 release not considered by the present model, such as bubble formation, $\bar{W}_{exergy,release}$ may become significant. The absence of exergy losses during CO_2 release is consistent with past work showing that CO_2 generation from acidified bicarbonate solutions is spontaneous relative to CO_2 capture into alkaline solutions.[50] Note that we also ignore exergy losses caused by temperature discontinuities within the electrolyte stemming from the reaction between CO_2 and OH^-.

In the presence of CO_2, there is significant hysteresis in the pH profile; this is because, although the pH increase during the charging half-cycle is insensitive to the presence of CO_2, the pH decrease upon discharge is buffered by (bi)carbonate.

Because the model keeps track of the cell's potential and current, as well as DIC, $[CO_2]$ in the CLE and P_{CO2} in the CLE's headspace over time, one can calculate not only the total work per mole of separated CO_2 but also the component of this work attributable to exergy losses, cell losses and $\bar{W}_{min,theor}$. This breakdown is shown in Figure 5 for the data in Figure 4,

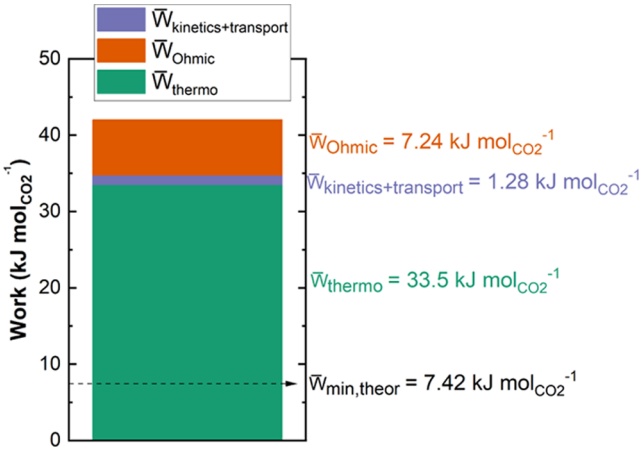

Figure 5. Total energetic cost of CO_2 separation in the baseline simulation in Figure 4 expressed as a sum of $\bar{W}_{thermo}$ (which includes exergy losses) and cell losses ($\bar{W}_{ohmic}$ + $\bar{W}_{kinetics+transport}$).

where cell losses are decomposed into a lumped contribution from charge transfer and mass transport losses and a second contribution from the Ohmic loss. $\bar{W}_{echem}$ was calculated according to

$$\bar{W}_{echem} = \frac{nF}{\Delta DIC_{released}} \oint E \, d\Psi \quad (6)$$

where ψ is the charge passed and $\Delta DIC_{released}$ is indicated in Figure 4c. Applying this equation to the data in Figure 4a,c yielded a value of 42.0 kJ $mol_{CO_2}^{-1}$. As calculated from eqs S13 and S17 using numerical integration, total exergy losses, $\bar{W}_{exergy,capture}$+ $\bar{W}_{exergy,release}$, amounted to 20.5 kJ $mol_{CO_2}^{-1}$.

Using the model's output, it is also possible to calculate the net rate of CO_2 removal from the inlet feed per geometric area of the cell (A_{geo}), ($\Delta DIC_{released} \times volume_{CLE}$)/($T_{cycle} \times A_{geo}$), denoted hereafter as CO_2 productivity (Φ_{CO_2}) in mol_{CO_2} m^{-2} h^{-1}. For the data in Figure 4, the Φ_{CO_2} value was 0.98 mol_{CO_2} m^{-2} h^{-1}. Our model therefore affords an approach for exploring relationships among exergy losses and the total

https://doi.org/10.1021/acssuschemeng.3c04867
ACS Sustainable Chem. Eng. 2023, 11, 16995−17005

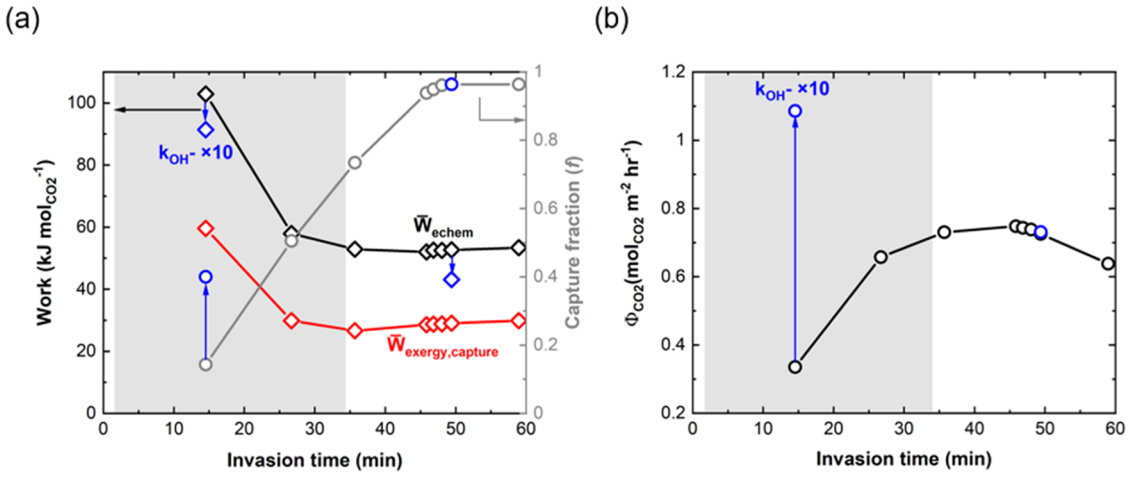

Figure 6. (a) Electrochemical work and capture fraction vs invasion time. (b) CO_2 productivity vs invasion time. Constant-current cycling results at 10 mA cm^{-2} account for 0 < $t_{invasion}$ < 45.7 min and constant-current constant-voltage cycling for 45.7 min < $t_{invasion}$ < 59 min where 0.1 mA cm^{-2} < j_{cutoff} < 5 mA cm^{-2} with $V_{invasion}$ = 200 mL and k_{OH^-} = 8500 M^{-1} s^{-1}. The estimated time scale for reactive capture of all of the CO_2 in the inlet is expected to lie within the gray zone in both plots. The blue data points correspond to k_{OH^-} = 85,000 M^{-1} s^{-1}.

energetic cost and rate of CO_2 separation. Leveraging this framework, we focus in the next section on assessing performance limits for pH-swing-driven CO_2 capture for a few application-oriented case studies.

Assessing Energetic Cost and Rate of CO_2 Capture in Application-Oriented Case Studies. Given the increasing uptake in stationary power generation systems of natural gas as a substitute fuel for coal, the baseline scenario in Figure 4 considered a CO_2 feed at 0.05 bar as representative of flue gas from a natural gas plant.[51] It did not consider a reduction in $P_{CO_2,inlet}$ as the CO_2 capture progressed. Nevertheless, an important practical criterion for point source capture applications such as flue gas capture is that a majority of the CO_2 in a given feed is removed.[28] We therefore also simulated CO_2 removal from a series of finite-sized gas inlets where inlet P_{CO_2} decreases during the capture step in proportion to the amount of CO_2 removed.

Figure S6a shows the energetic cost of CO_2 capture from a 0.05 bar input feed and release to 1 bar as the size of the gas inlet decreases and the fraction of CO_2 captured (denoted hereafter as f) increases. The total energetic cost increases significantly as the input size decreases, from 42.0 kJ mol$_{CO_2}^{-1}$ for an inlet of infinite size (i.e., a fixed $P_{CO_2,inlet}$ and f = 0), to 107 kJ mol$_{CO_2}^{-1}$ for a 50 mL inlet reservoir, where f is 0.99. The energetic cost mainly comprises the exergy loss from CO_2 capture, which would be expected to increase with a decrease in the gas inlet size and thus a decrease in average $P_{CO_2,inlet}$. The increase in the energetic cost for CO_2 capture with increasing f corresponds to a decrease in Φ_{CO_2} from 0.98 mol$_{CO_2}$ m^{-2} h^{-1} for the infinitely large inlet to 0.20 mol$_{CO_2}$ m^{-2} h^{-1} for the 50 mL inlet (Figure S6b). Again, this result is reasonable because as P_{CO_2} in the inlet feed decreases, so does the rate of CO_2 capture according to eq 4. A notable implication of this finding is that lab-scale electrochemical measurements of flue gas capture of CO_2 in which the inlet P_{CO_2} is fixed, or exhibits a negligible decrease, might severely underestimate energy penalties that would be incurred in practical situations where near-complete extraction of CO_2 from a given feed is desired.

Figure S7a shows the effect of changing the applied current density during CCCV cycling on the energetic cost of the CO_2 concentration for an inlet of 200 mL and initial inlet P_{CO_2} of 0.05 bar. The total energetic cost increases from 41.2 kJ mol$_{CO_2}^{-1}$ at 5 mA cm^{-2} to 105 kJ mol$_{CO_2}^{-1}$ at 50 mA cm^{-2}, and 137 kJ mol$_{CO_2}^{-1}$ at 100 mA cm^{-2}. Clearly, the increase is mainly attributable to an increase in cell (especially Ohmic) losses rather than exergy losses. Corresponding to this increase in energetic cost is an increase in Φ_{CO_2} from 0.37 mol$_{CO_2}$ m^{-2} h^{-1} at 5 mA cm^{-2} to 2.6 mol$_{CO_2}$ m^{-2} h^{-1} at 50 mA cm^{-2}, and 3.3 mol$_{CO_2}$ m^{-2} h^{-1} at 100 mA cm^{-2} (Figure S7b). This increase in Φ_{CO_2} originates from the shorter cycle periods associated with the increasing current density. Despite the shorter cycle periods, CO_2 uptake approaches completion (f = 0.97) within the range of current densities tested because of rapid reactive capture of CO_2 relative to the cycle period, which is lengthened by the inclusion of a CV step. In the absence of this CV step (i.e., constant-current cycling), f decreases to 0.30 at the highest current density of 50 mA cm^{-2} (Figure S8), where the cycle period is apparently too short for CO_2 removal to approach completion. Note that for constant-current (CC) cycling at 5 mA cm^{-2}, the cycle period is long enough for the CO_2 invasion to go to completion (f = 0.97), with an energetic cost of 40.8 kJ mol$_{CO_2}^{-1}$ and Φ_{CO_2} of 0.38 mol$_{CO_2}$ m^{-2} h^{-1}, virtually identical to the CCCV analogue shown in Figure S7.

Figure 6 shows that the above relationships among f, Φ_{CO_2}, and $\bar{W}_{echem}$ can be understood in terms of the difference between the time allotted for deacidification/CO_2 invasion (during CCCV and CV cycling), and that required for reactive CO_2 capture. As shown in Figure 6a, the longer the invasion time, the more gas- and solution-phases of CO_2 approach equilibrium, leading to higher f and lower $\bar{W}_{exergy,capture}$ ($\bar{W}_{exergy,release}$ is negligible in all cases). There is a prominent "knee" in the f vs invasion time profile around 45−50 min, after which f and $\bar{W}_{exergy,capture}$ approach 0.99 and 29.8 kJ mol$_{CO_2}^{-1}$, respectively. We hypothesize that this knee occurs where the duration of the deacidification/CO_2 invasion half-

https://doi.org/10.1021/acssuschemeng.3c04867
ACS Sustainable Chem. Eng. 2023, 11, 16995−17005

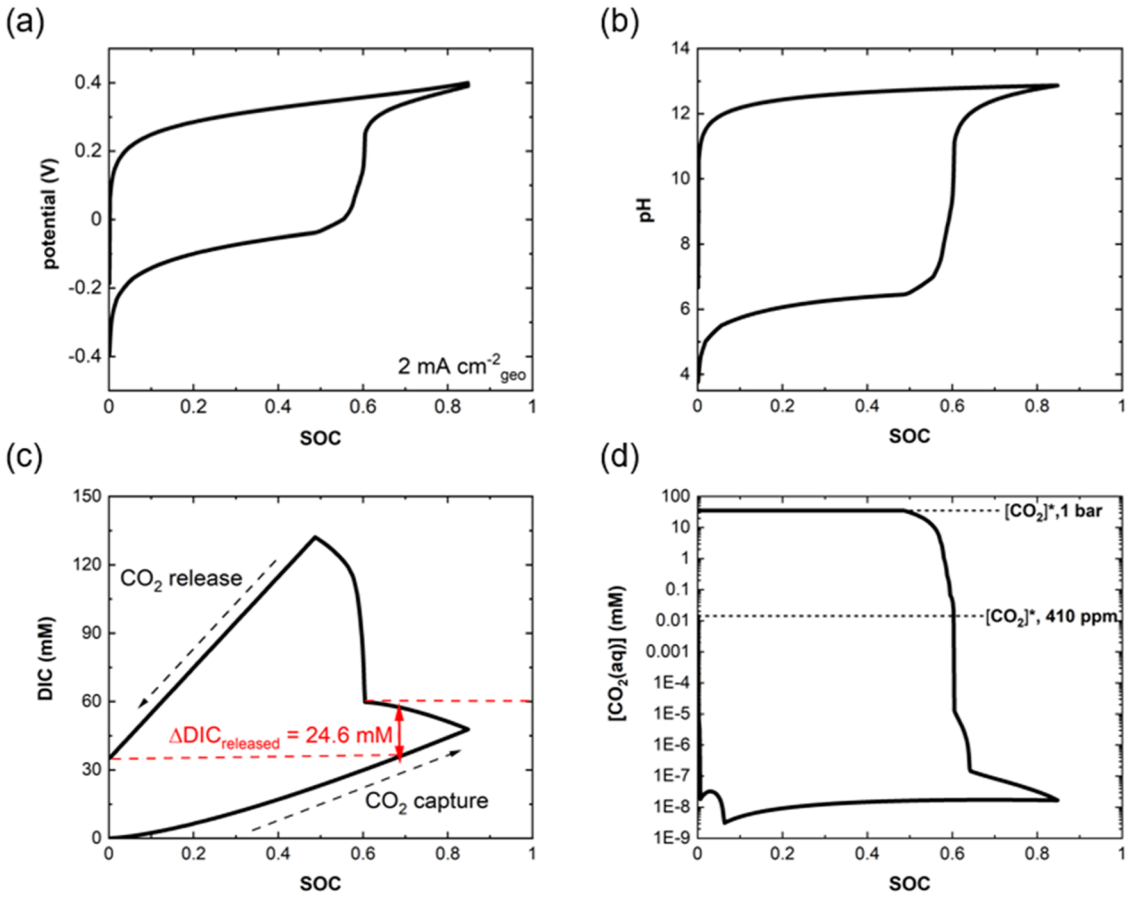

Figure 7. (a) Potential, (b) pH, (c) DIC, and (d) $[CO_2]$ vs SOC for CCCV cycling at 2 mA cm^{-2} with $P_{CO_2,inlet}$ = 410 ppm inlet and $P_{CO_2,exit}$ = 1 bar.

cycle ($t_{invasion}$) begins to exceed the time required for reactive capture of CO_2 ($t_{capture}$). As $t_{capture}$ exceeds the invasion time, $[CO_2]$ progressively subceeds $[CO_2]^*$ during the invasion step, causing $\bar{W}_{exergy,capture}$ to increase and f to decrease. $t_{capture}$ can be estimated by dividing the initial amount of CO_2 in the 200 mL inlet gas reservoir (in moles) by $R_{capture}$ from eq 4. However, because $P_{CO_2,inlet}$ (and thus $[CO_2]^*$) and $[OH^-]$ can decrease during CO_2 capture, $R_{capture}$ will not necessarily be fixed. We therefore calculated a range for $t_{capture}$ based on two extreme cases: one, representing a scenario with a small change in the pH of the CLE, where average $P_{CO_2,inlet}$ and $[OH^-]$ are 0.025 bar and 0.08 M, respectively, and another scenario where average $P_{CO_2,inlet}$ and $[OH^-]$ are 0.0075 bar and 2.40 mM. This calculation yields a $t_{capture}$ range of 1.77−34.1 min (see gray zones in Figure 6), with the upper limit preceding the occurrence of the knee by about 10 min.

The competition between cycling and reactive capture time scales also governs the Φ_{CO_2} vs invasion time profile (Figure 6b), which exhibits a maximum around ∼45 min. Below this point, there is progressively less time for the complete removal of CO_2; above it, the increasing cycle period induces no additional CO_2 capture as $f \sim 1$.

These results provide some guidance on where homogeneous catalysis is likely to be effective in improving the rate and energetic cost of CO_2 separation. Because catalysis reduces the time-averaged difference between $[CO_2]$ and $[CO_2]^*$, it will be more effective in increasing Φ_{CO_2} and decreasing $\bar{W}_{exergy,capture}$ as the absolute value of $[CO_2] - [CO_2]^*$ increases, which occurs as invasion durations fall short of the $t_{capture}$ range indicated in Figure 6. To verify this, we quantified the change in Φ_{CO_2}, $\bar{W}_{echem}$, and $\bar{W}_{exergy,capture}$ brought about by a 10-fold increase in k_{OH} (from 8,500 to 85,000 M^{-1} s^{-1}) for CCCV cycling at 10 and 20 mA cm^{-2} (blue data points in Figure 6a,b). These current densities resulted in invasion half-cycle periods of 49.4 and 14.5 min, respectively, i.e., at high and low $t_{invasion}$. In the former case, where $t_{invasion} > t_{capture}$, $\bar{W}_{echem}$ decreased modestly, from 52.7 to 43.1 kJ $mol_{CO_2}^{-1}$, whereas Φ_{CO_2} was virtually identical to its uncatalyzed analogue (blue arrows in Figure 6a,b). In the latter case, there was a slightly larger decrease in $\bar{W}_{echem}$ from 103 to 91.4 kJ $mol_{CO_2}^{-1}$, and a dramatic 3-fold increase in Φ_{CO_2} from 0.34 to 1.1 mol m^{-2} h^{-1}, in line with our expectations.

We also investigated the energetic cost of electrochemical concentration of CO_2 from its partial pressure in atmosphere (410 ppm) to 1 bar, as DAC is increasingly being seen as an important option in our portfolio of climate stabilization strategies.[3] Figure 7 reports potential, pH, DIC, and $[CO_2]$ over a CO_2-concentrating cycle where $P_{CO_2,inlet}$ was fixed at 410 ppm. All other parameters from the baseline scenario in Figure 4 were retained, except for the current density of 10 mA cm^{-2}. Cycling at 10 mA cm^{-2} in 410 ppm afforded such a low cycle period (compared to the time scale required for DAC) that DIC at the end of invasion (1.28 mM) was lower than $[CO_2]^*$ at 1 bar (35 mM), making outgassing thermodynamically

https://doi.org/10.1021/acssuschemeng.3c04867
ACS Sustainable Chem. Eng. 2023, 11, 16995−17005

impossible (data not shown). We therefore reduced the current density to 2 mA cm^{-2}. Under these conditions, DIC at the end of the charging half-cycle (Figure 7c) was 47.9 mM, and $\bar{W}_{echem}$ and Φ_{CO_2} were 142 kJ $mol_{CO_2}^{-1}$ and 0.07 mol_{CO_2} m^{-2} h^{-1}, respectively. Out of the total of 142 kJ $mol_{CO_2}^{-1}$, about 133 kJ $mol_{CO_2}^{-1}$ is attributable to $\bar{W}_{thermo}$, which is reasonable given that DAC has slow kinetics. The slow kinetics leads to a $[CO_2]$ that is lower than its equilibrium value at 410 ppm before outgassing is initiated, and results in a higher $\bar{W}_{thermo}$ than would be inferred from Figure 2, where equilibrium is assumed. Therefore, some combination of a higher $A_{contact}$ and an increase in CO_2 hydroxylation/hydration kinetics (e.g., via homogeneous catalysis, or a much higher $[Q_0]$) would further improve $\bar{W}_{echem}$ and Φ_{CO_2}.

Experimental Implications. The results from the above zero-dimensional model and exergy loss analysis have several implications for electrochemical CO_2 capture research and its further development for industrial application.

First, they provide a framework for understanding how thermodynamic and kinetic factors (exergy and cell losses) compose the measured energy inputs in the electrochemical CO_2 separation processes. Direct comparison between energetic costs for PCET-/pH-swing-driven CO_2 separation in previous studies[10,11,25] and that of our model is not possible at present, in part because several parameters required to describe CO_2 capture/release kinetics (e.g., $A_{contact}$, k_L) are unknown, as is the pH dependence of redox kinetics and Ohmic resistance. It is nonetheless encouraging that the range of energetic costs yielded by our simulations (40−140 kJ $mol_{CO_2}^{-1}$ between 5 and 100 mA cm^{-2} for capture from 0.05 bar, see Figure S7) is in reasonably good agreement with that from a recent experimental study[25] (60−150 kJ $mol_{CO_2}^{-1}$ between 25 and 150 mA cm^{-2} for capture from 0.1 bar). The model may be modified to simulate and lend insight into energetic costs for NB-driven capture of CO_2. However, although there is considerable literature on CO_2 binding constants,[19,44,52] relatively little is known about the rate constant(s) of adduct formation between CO_2 and redox-active nucleophiles,[41] which is a critical input. It is, nevertheless, worth noting that many of these unknown parameters are measurable. $A_{contact}$ and k_L can be measured using string-of-disks or string-of-sphere contactors;[49] rate constants for CO_2 binding, and the pH dependence of redox kinetics and cell resistance can likewise be measured using standard electroanalytical techniques such as voltammetry and impedance spectroscopy.[53−55]

Second, because $\bar{W}_{thermo}$ and exergy loss are functions of $[CO_2]$, it is possible, in principle, to experimentally assess their influence on $\bar{W}_{echem}$ if the trajectory of $[CO_2]$ within a cycle is known. Direct measurements of solution-phase CO_2 have not been attempted in the electrochemical CO_2 separation literature, but are experimentally accessible, using a Severinghaus electrode,[56] for instance. In future work, combining real-time measurements of $[CO_2]$ with those of P_{CO_2} and DIC (e.g., obtained indirectly via pH measurements, or more directly, from total carbon analysis), will enable straightforward assessment of many of the trends simulated in this work, e.g., between invasion time and CO_2 throughput (Figure 6b), invasion time and total work input (Figure 6a), and the impact of homogeneous catalysis on both (Figure 6a,b).

Third, given its relevance to point source capture, it would be important for future experimental studies to mimic near-complete removal of CO_2 from simulated flue gas feeds, as the decrease in $P_{CO_2,inlet}$ accompanying such removal can dramatically increase $\bar{W}_{echem}$. To our knowledge, no experimental studies have examined the impact of a decreasing $P_{CO_2,inlet}$ on $\bar{W}_{echem}$, and only one has systematically examined $\bar{W}_{echem}$ for $P_{CO_2,exit}/P_{CO_2,inlet}$ ratios greater than 1.[25]

Finally, the model and exergy loss analysis presented here can inform techno-economic assessment of the lowest possible cost of CO_2 captured/avoided (in \$ $ton_{CO_2}^{-1}$) in industrial or other real-world contexts. For instance, for a given rate of CO_2 emitted from a fossil plant (in mol_{CO_2} h^{-1}) and a desired degree of extraction (f), one could calculate the optimal number of electrochemical cells to deploy based on the capital and operating cost of each cell and the cost of electricity/fuel. Trade-offs/relationships between the levelized CO_2 cost and f, $\bar{W}_{echem}$, or throughput can also be quantified.

SUMMARY

The minimum work thermodynamically required to execute electrochemical CO_2 separation is the sum of the net increase in the level of CO_2 exergy and all exergy losses incurred upon entry of CO_2 into and release from the electrolyte. We computed these exergy losses based on the trajectory of $[CO_2]$ in the electrolyte and the partial pressure of CO_2 in the gas phase and showed that they imposed constraints on the molecular properties required to enact CO_2 separation via PCET-driven pH-swing and direct binding of CO_2 to a nucleophilic charge carrier. By modifying a zero-dimensional electrochemical model we previously developed for simulating capacity fade in organic flow cells,[24] we have also shown how kinetic losses (arising from interfacial charge transfer, Ohmic resistances, and mass transport) combine with these exergy losses and compose the total work for pH-swing-based CO_2 concentration driven by PCET. We explored the effect of varying various process and electrochemical parameters, such as the inlet CO_2 reservoir size (Figure S6), current density (Figure S7), and the rate constant of CO_2 hydroxylation (k_{OH^-}) (Figure 6), on the energetic cost ($\bar{W}_{echem}$) and rate (Φ_{CO_2}) of CO_2 separation, as well as the fraction of CO_2 removed from the inlet (f). A key insight from our investigations is that the difference between the CO_2 invasion timescale ($t_{invasion}$) and the time required for reactive capture of CO_2 ($t_{capture}$) governs the trade-off/relationship between Φ_{CO_2} and $\bar{W}_{echem}$. When the two timescales are comparable, Φ_{CO_2} is optimally high. But as $t_{capture}$ exceeds $t_{invasion}$, f and Φ_{CO_2} decrease, whereas $\bar{W}_{echem}$ increases due to increasing exergy losses during CO_2 capture. Under such conditions, increasing k_{OH^-} substantially increases f and Φ_{CO_2} (Figure 6). This result has particularly important implications for the capture of CO_2 from point sources, where high values of f and Φ_{CO_2} are desired. Lastly, we showed that pH-swing-driven CO_2 capture from air is possible at $\bar{W}_{echem}$ and Φ_{CO_2} values of 142 kJ $mol_{CO_2}^{-1}$ and 0.07 mol_{CO_2} m^{-2} h^{-1}, respectively, although further improvements are feasible.

https://doi.org/10.1021/acssuschemeng.3c04867
ACS Sustainable Chem. Eng. 2023, 11, 16995−17005

■ ASSOCIATED CONTENT

Supporting Information

The Supporting Information is available free of charge at https://pubs.acs.org/doi/10.1021/acssuschemeng.3c04867.

Detailed derivations of equations describing exergy loss analysis and description of zero-dimensional model; full derivations of the exergy loss equations; background physics and chemistry of pH swing and NB CO_2 capture models; and exergy loss and 0-D model additional results (PDF)

■ AUTHOR INFORMATION

Corresponding Author

David G. Kwabi − *Department of Mechanical Engineering, University of Michigan, Ann Arbor, Michigan 48109, United States;* orcid.org/0000-0003-3663-8789; Email: dkwabi@umich.edu

Authors

Fawaz Ali − *Department of Mechanical Engineering, University of Michigan, Ann Arbor, Michigan 48109, United States*

Sanat Modak − *Department of Mechanical Engineering, University of Michigan, Ann Arbor, Michigan 48109, United States;* orcid.org/0000-0002-3822-8794

Complete contact information is available at: https://pubs.acs.org/10.1021/acssuschemeng.3c04867

Author Contributions

The manuscript was written through contributions of all authors. All authors have given approval to the final version of the manuscript.

Notes

The authors declare no competing financial interest.

■ ACKNOWLEDGMENTS

This work was funded by the National Science Foundation under award number 2045032.

■ LIST OF ABBREVIATIONS

CCCV	constant-current, constant-voltage
CV	constant voltage
CLE	capacity-limiting electrolyte
DAC	direct air capture
DIC	dissolved inorganic carbon
IU	invasion underpressure
NB	nucleophilic binding
NCLE	noncapacity-limiting electrolyte
OP	outgassing overpressure
PCET	proton-coupled electron transfer
SOC	state of charge
TA	total alkalinity

■ ADDITIONAL NOTE

[a]This extra work may also be considered an exergy loss, but we reserve the term in this study for the chemical/stream exergy losses from CO_2 capture and release.

■ REFERENCES

(1) *Climate Change 2014: Synthesis Report* IPCC: Geneva, Switzerland; 2014.

(2) *IPCC Special Report on Carbon Dioxide Capture and Storage* IPCC, Cambridge University Press, Cambridge: United Kingdom and New York, NY; 2005.

(3) *Negative Emissions Technologies and Reliable Sequestration: A Research Agenda* National Academies of Sciences, Engineering and Medicine: Washington, DC; 2019.

(4) Lackner, K. S.; Brennan, S.; Matter, J. M.; Park, A.-H. A.; Wright, A.; van der Zwaan, B. The urgency of the development of CO2 capture from ambient air. *Proc. Natl. Acad. Sci. U.S.A.* **2012**, *109*, 13156−13162.

(5) Lackner, K. S.; Grimes, P.; Ziock, H. J. *Carbon Dioxide Extraction from Air: Is it an Option?*, Proceedings of the 24th Annual Technical Conference on Coal Utilization and Fuel Systems; Clearwater, FL, 1999; pp 885−896.

(6) Li, K.; Cousins, A.; Yu, H.; Feron, P.; Tade, M.; Luo, W.; Chen, J. Systematic study of aqueous monoethanolamine-based CO2 capture process: model development and process improvement. *Energy Sci. Eng.* **2016**, *4* (1), 23−39.

(7) Keith, D. W.; Holmes, G.; St Angelo, D.; Heidel, K. A Process for Capturing CO2 from the Atmosphere. *Joule* **2018**, *2*, 1573−1594, DOI: 10.1016/j.joule.2018.05.006.

(8) House, K. Z.; Baclig, A. C.; Ranjan, M.; van Nierop, E. A.; Wilcox, J.; Herzog, H. J. Economic and energetic analysis of capturing CO2 from ambient air. *Proc. Natl. Acad. Sci. U.S.A.* **2011**, *108* (51), 20428−20433.

(9) Renfrew, S. E.; Starr, D. E.; Strasser, P. Electrochemical Approaches toward CO2 Capture and Concentration. *ACS Catal.* **2020**, *10* (21), 13058−13074.

(10) Jin, S.; Wu, M.; Gordon, R. G.; Aziz, M. J.; Kwabi, D. G. pH swing cycle for CO2 capture electrochemically driven through proton-coupled electron transfer. *Energy Environ. Sci.* **2020**, *13*, 3706.

(11) Xie, H.; Wu, Y.; Liu, T.; Wang, F.; Chen, B.; Liang, B. Low-energy-consumption electrochemical CO2 capture driven by biomimetic phenazine derivatives redox medium. *Appl. Energy* **2020**, *259*, No. 114119.

(12) Rahimi, M.; Catalini, G.; Hariharan, S.; Wang, M.; Puccini, M.; Hatton, T. A. Carbon Dioxide Capture Using an Electrochemically Driven Proton Concentration Process. *Cell Rep. Phys. Sci.* **2020**, *1* (4), No. 100033.

(13) Rahimi, M.; Catalini, G.; Puccini, M.; Hatton, T. A. Bench-scale demonstration of CO2 capture with an electrochemically driven proton concentration process. *RSC Adv.* **2020**, *10* (29), 16832−16843.

(14) Kim, S.; Nitzsche, M.; Rufer, S. B.; Lake, J. R.; Varanasi, K. K.; Hatton, T. A. Asymmetric chloride-mediated electrochemical process for CO2 removal from oceanwater. *Energy Environ. Sci.* **2023**, *16*, 2030.

(15) Seo, H.; Hatton, T. A. Electrochemical direct air capture of CO2 using neutral red as reversible redox-active material. *Nat. Commun.* **2023**, *14* (1), No. 313.

(16) Voskian, S.; Hatton, T. A. Faradaic electro-swing reactive adsorption for CO2 capture. *Energy Environ. Sci.* **2019**, *12* (12), 3530−3547.

(17) Diederichsen, K. M.; Liu, Y.; Ozbek, N.; Seo, H.; Hatton, T. A. Toward solvent-free continuous-flow electrochemically mediated carbon capture with high-concentration liquid quinone chemistry. *Joule* **2022**, *6*, 221.

(18) Seo, H.; Rahimi, M.; Hatton, T. A. Electrochemical Carbon Dioxide Capture and Release with a Redox-Active Amine. *J. Am. Chem. Soc.* **2022**, *144*, 2164.

(19) Petersen, H. A.; Alherz, A. W.; Stinson, T. A.; Huntzinger, C. G.; Musgrave, C. B.; Luca, O. R. Predictive energetic tuning of C-Nucleophiles for the electrochemical capture of carbon dioxide. *iScience* **2022**, *25* (4), No. 103997.

(20) Wang, M.; Hariharan, S.; Shaw, R. A.; Hatton, T. A. Energetics of electrochemically mediated amine regeneration process for flue gas CO2 capture. *Int. J. Greenhouse Gas Control* **2019**, *82*, 48−58.

(21) Shaw, R. A.; Hatton, T. A. Electrochemical CO2 capture thermodynamics. *Int. J. Greenhouse Gas Control* **2020**, *95*, No. 102878.

(22) Petersen, H. A.; Luca, O. R. Application-specific thermodynamic favorability zones for direct air capture of carbon dioxide. *Phys. Chem. Chem. Phys.* **2021**, *23* (22), 12533−12536.
(23) Clarke, L. E.; Leonard, M. E.; Hatton, T. A.; Brushett, F. R. Thermodynamic Modeling of CO2 Separation Systems with Soluble, Redox-Active Capture Species. *Ind. Eng. Chem. Res.* **2022**, *61*, 10531.
(24) Modak, S.; Kwabi, D. G. A Zero-Dimensional Model for Electrochemical Behavior and Capacity Retention in Organic Flow Cells. *J. Electrochem. Soc.* **2021**, *168* (8), No. 080528.
(25) Jin, S.; Wu, M.; Jing, Y.; Gordon, R. G.; Aziz, M. J. Low energy carbon capture via electrochemically induced pH swing with electrochemical rebalancing. *Nat. Commun.* **2022**, *13* (1), No. 2140.
(26) Chehayeb, K. M.; Lienhard, J. H. Entropy generation analysis of electrodialysis. *Desalination* **2017**, *413*, 184−198.
(27) Nemani, V. P.; Smith, K. C. Assignment of energy loss contributions in redox flow batteries using exergy destruction analysis. *J. Power Sources* **2020**, *447*, No. 227371.
(28) Lackner, K. S. The thermodynamics of direct air capture of carbon dioxide. *Energy* **2013**, *50*, 38−46.
(29) Hoober-Burkhardt, L.; Krishnamoorthy, S.; Yang, B.; Murali, A.; Nirmalchandar, A.; Surya Prakash, G. K.; Narayanan, S. R. A new Michael-reaction-resistant benzoquinone for aqueous organic redox flow batteries. *J. Electrochem. Soc.* **2017**, *164* (4), A600−A607.
(30) Huang, C.; Liu, C.; Wu, K.; Yue, H.; Tang, S.; Lu, H.; Liang, B. CO2 Capture from Flue Gas Using an Electrochemically Reversible Hydroquinone/Quinone Solution. *Energy Fuels* **2019**, *33*, 3380.
(31) Luo, L.; Hou, L.; Liu, Y.; Wu, K.; Zhu, Y.; Lu, H.; Liang, B. Regeneration of Na2Q in an Electrochemical CO2 Capture System. *Energy Fuels* **2021**, *35* (15), 12260−12269.
(32) Yang, B.; Hoober-Burkhardt, L.; Krishnamoorthy, S.; Murali, A.; Surya Prakash, G. K.; Narayanan, S. R. High-Performance Aqueous Organic Flow Battery with Quinone-Based Redox Couples at Both Electrodes. *J. Electrochem. Soc.* **2016**, *163*, A1442−A1449.
(33) Wu, M.; Jing, Y.; Wong, A. A.; Fell, E. M.; Jin, S.; Tang, Z.; Gordon, R. G.; Aziz, M. J. Extremely Stable Anthraquinone Negolytes Synthesized from Common Precursors. *Chem* **2020**, *6*, 1432.
(34) Jing, Y.; Fell, E. M.; Wu, M.; Jin, S.; Ji, Y.; Pollack, D. A.; Tang, Z.; Ding, D.; Bahari, M.; Goulet, M.; Tsukamoto, T.; Gordon, R. G.; Aziz, M. J. Anthraquinone Flow Battery Reactants with Non-hydrolyzable Water-Solubilizing Chains Introduced via a Generic Cross-Coupling Method. *ACS Energy Lett.* **2022**, *7*, 226−235.
(35) Gaudin, T.; Aubry, J.-M. Prediction of Pourbaix diagrams of quinones for redox flow battery by COSMO-RS. *J. Energy Storage* **2022**, *49*, No. 104152.
(36) Pang, S.; Wang, X.; Wang, P.; Ji, Y. Biomimetic Amino Acid Functionalized Phenazine Flow Batteries with Long Lifetime at Near-Neutral pH. *Angew. Chem., Int. Ed.* **2021**, *60*, 5289.
(37) Hollas, A.; Wei, X.; Murugesan, V.; Nie, Z.; Li, B.; Reed, D.; Liu, J.; Sprenkle, V.; Wang, W. A biomimetic high-capacity phenazine-based anolyte for aqueous organic redox flow batteries. *Nat. Energy* **2018**, *3* (6), 508−514.
(38) Xu, J.; Pang, S.; Wang, X.; Wang, P.; Ji, Y. Ultrastable aqueous phenazine flow batteries with high capacity operated at elevated temperatures. *Joule* **2021**, *5* (9), 2437−2449.
(39) Fujita, E.; Creutz, C.; Sutin, N.; Szalda, D. J. Carbon dioxide activation by cobalt(I) macrocycles: factors affecting carbon dioxide and carbon monoxide binding. *J. Am. Chem. Soc.* **1991**, *113* (1), 343−353.
(40) Scovazzo, P.; Poshusta, J.; DuBois, D.; Koval, C.; Noble, R. Electrochemical Separation and Concentration of < 1% Carbon Dioxide from Nitrogen. *J. Electrochem. Soc.* **2003**, *150* (5), D91.
(41) Li, X.; Zhao, X.; Liu, Y.; Hatton, T. A.; Liu, Y. Redox-tunable Lewis bases for electrochemical carbon dioxide capture. *Nat. Energy* **2022**, *7*, 1065.
(42) DuBois, D. L.; Miedaner, A.; Bell, W.; Smart, J. C. Electrochemical Concentration of Carbon Dioxide. In *Electrochemical and Electrocatalytic Reactions of Carbon Dioxide*; Sullivan, B. P., Ed.; Elsevier, 1993; pp 94−117.
(43) Schmidt, M. H.; Miskelly, G. M.; Lewis, N. S. Effects of redox potential, steric configuration, solvent, and alkali metal cations on the binding of carbon dioxide to cobalt(I) and nickel(I) macrocycles. *J. Am. Chem. Soc.* **1990**, *112* (9), 3420−3426.
(44) Barlow, J. M.; Yang, J. Y. Oxygen-Stable Electrochemical CO2 Capture and Concentration with Quinones Using Alcohol Additives. *J. Am. Chem. Soc.* **2022**, *144*, 14161.
(45) Bard, A. J.; Faulkner, L. R. *Electrochemical Methods: Fundamentals and Applications*, 2nd ed.; Wiley: New York, 2001; pp 18−35.
(46) Zeebe, R. E.; Wolf-Gladrow, D. *CO2 in Seawater: Equilibrium, Kinetics, Isotopes*; Elsevier: Amsterdam, 2005; pp 27−50.
(47) Mahmoudkhani, M.; Keith, D. W. Low-energy sodium hydroxide recovery for CO2 capture from atmospheric air—Thermodynamic analysis. *Int. J. Greenhouse Gas Control* **2009**, *3* (4), 376−384.
(48) Holmes, G.; Keith, D. W. An air-liquid contactor for large-scale capture of CO2 from air. *Philos. Trans. R. Soc., A* **2012**, *370* (1974), 4380−4403.
(49) Danckwerts, P. V. *Gas-Liquid Reactions*; McGraw-Hill Book Co., 1970; pp 38−251.
(50) Schulz, K. G.; Riebesell, U.; Rost, B.; Thoms, S.; Zeebe, R. E. Determination of the rate constants for the carbon dioxide to bicarbonate inter-conversion in pH-buffered seawater systems. *Mar. Chem.* **2006**, *100* (1−2), 53−65.
(51) Albertus, P.; Manser, J. S.; Litzelman, S. Long-Duration Electricity Storage Applications, Economics, and Technologies. *Joule* **2020**, *4* (1), 21−32.
(52) Alherz, A. W.; Petersen, H. A.; Singstock, N. R.; Sur, S. N.; Musgrave, C. B.; Luca, O. R. Predictive energetic tuning of quinoid O-nucleophiles for the electrochemical capture of carbon dioxide. *Energy Advances* **2022**, *1*, 900. 10.1039/D2YA00114D
(53) Savéant, J. M. *Elements of Molecular and Biomolecular Electrochemistry: An Electrochemical Approach to Electron Transfer Chemistry*; Wiley: New York, 2006; pp 1−75.
(54) Yang, S.; Chen, Q. Quantifying Electron Transfer Kinetics on Porous Carbon Electrodes for Redox Flow Batteries. *J. Electrochem. Soc.* **2020**, *167* (16), No. 160501.
(55) Sawant, T. V.; Yim, C. S.; Henry, T. J.; Miller, D. M.; McKone, J. R. Harnessing Interfacial Electron Transfer in Redox Flow Batteries. *Joule* **2021**, *5*, 360.
(56) Severinghaus, J. W.; Bradley, A. F. Electrodes for Blood pO2 and pCO2 Determination. *J. Appl. Physiol.* **1958**, *13* (3), 515−520.

https://doi.org/10.1021/acssuschemeng.3c04867
ACS Sustainable Chem. Eng. 2023, 11, 16995−17005